

Interplay of Kondo effect and strong spin-orbit coupling in multi-hole ultraclean carbon nanotubes

J. P. Cleuziou, N. V. N'Guyen, S. Florens, and W. Wernsdorfer
Institut Néel, CNRS et Université Joseph Fourier BP 166, 38042 Grenoble Cedex 9, France

We report on cotunneling spectroscopy magnetoconductance measurements of multi-hole ultraclean carbon nanotube quantum dots in the SU(4) Kondo regime with strong spin-orbit coupling. Successive shells show a gradual weakening of the Kondo effect with respect to the spin-orbital splittings, leading to an evolution from SU(4) to SU(2) symmetry with a suppressed conductance at half shell filling. The extracted energy level spectrum, overall consistent with negligible disorder in the nanotube, shows in the half filled case large renormalizations due to Coulombian effects.

The interplay between electron orbital and spin degrees of freedom in nanostructures is the current subject of intense studies. In this context, carbon nanotubes (CNTs) have attracted a considerable interest due to quite unique electronic properties [1] making them attractive candidates for spintronics devices [2, 3] and spin qubits [4, 5]. In particular, single-electron tunneling spectroscopy in ultraclean CNT devices [6, 7] has shown the important role of the curvature induced spin-orbit interaction (SOI) [8, 9], which partially splits the fourfold degenerate electron shell level structure by an effective energy gap Δ_{SO} . This result was confirmed in the many electron regime, including a significant disorder induced orbital mixing $\Delta_{KK'} \gg \Delta_{SO}$ [10].

On the other hand, it is well established that quantum dots with sufficiently strong tunnel couplings to the metallic leads exhibit rich Kondo physics [11]. In particular, for a CNT having the fourfold level degeneracy, the dot spin and orbital degrees of freedom become strongly coupled to those of the leads (assuming conserved orbital quantum numbers during the tunneling processes), thereby forming a highly entangled SU(4) Kondo ground state [12, 13] with an enhanced Kondo temperature T_K [14, 15]. By taking into account the SOI in the CNT energy spectrum, a mutual interplay between the SOI and Kondo correlations is expected [16, 17], resulting in a crossover from SU(4) [15, 18] ($k_B T_K \gg \Delta_{SO}$) to more conventional SU(2) Kondo effects [19] ($k_B T_K \ll \Delta_{SO}$) at zero magnetic field. While some deviations of SU(4) Kondo physics related to the SOI have been discussed theoretically [16] in connexion to previous experiments [14, 15], the full detailed experimental study of disorder-free CNT quantum dots in the Kondo regime with well-resolved SOI split energy spectrum is still missing.

In this Letter, we study by means of cotunneling magneto-spectroscopy under a parallel magnetic field B_{\parallel} (see Ref. [20], section 1.2 for the actual alignment relative to the CNT axis in Fig. 1(a)) the orbital structure and the Kondo effects in an ultraclean CNT quantum dot, with an energy level structure dominated by the SOI ($\Delta_{SO} \gg \Delta_{KK'}$). This complements recent studies performed in the sequential tunneling regime where Kondo physics was absent [6, 7], while previous cotun-

neling measurements were made on disorder-dominated samples [10, 21]. One striking finding is the strong renormalization of the effective SOI splitting at half shell filling, denoted Δ_{SO}^* (see below), resulting systematically in very different SOI energy scales for odd and even hole numbers ($\Delta_{SO}^* > \Delta_{SO}$). In the weak Kondo regime ($k_B T_K \ll \Delta_{SO}^*$), the Kondo effect is quenched for an even charge on the dot, as predicted theoretically [16]. As the dot tunnel coupling is then increased with larger gate voltages, the Kondo effect is greatly enhanced and Kondo correlations tend to restore the full SU(4) Kondo symmetry [14, 15]. For intermediate gate voltages, we are thus able to study the regime of comparable Kondo and orbital energy scales ($k_B T_K \simeq \Delta_{SO}^*$) where the orbital structure competes with SU(4) Kondo physics [16].

The quantum dot studied here is based on an ultraclean CNT [6] grown on top of predefined source (S) and

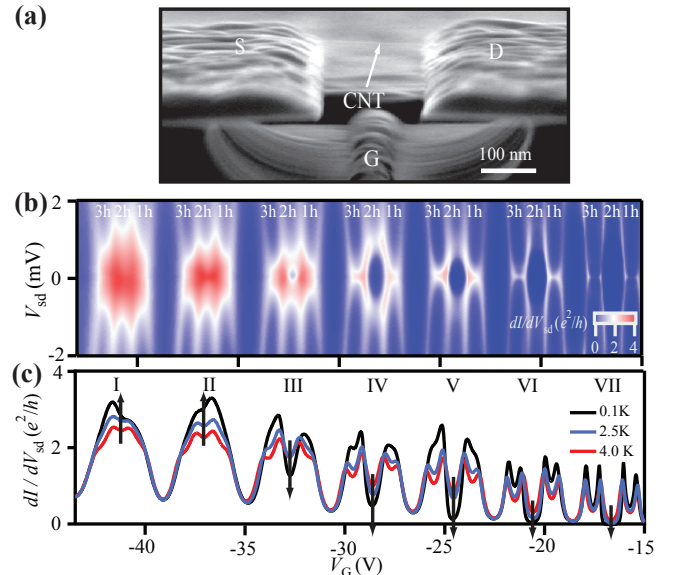


FIG. 1. (color online). (a) Scanning electron microscopy of an ultraclean nanotube device similar to the one used in the measurements. (b) Differential conductance map dI/dV_{sd} versus gate voltage V_G and bias voltage V_{sd} at $T \approx 30$ mK. (c) Linear differential conductance versus V_G , measured at different temperatures.

drain (D) Pt metal contacts and suspended over a gate electrode [22] (Fig. 1(a)). A different device, showing similar physics, is further discussed in Ref. [20], section 2. Applying a voltage on the gate shifts the chemical potential of the single CNT quantum dot (≈ 200 -nm-long) [23], as depicted in the device stability diagram of Fig. 1(b). As negative V_G shifts the Fermi level below the edge of the nanotube bandgap ($E_g \approx 300$ meV), additional holes (typically from 10 to 40 here) are subsequently added to the CNT valence band and the conductance displays a series of Coulomb peaks for each additional hole, connected by either Coulomb blockade valleys or Kondo ridges at zero bias [19]. The four hole periodicity in the charge stability diagram of Fig. 1(b) demonstrates that the energy level spectrum consists of four-fold nearly degenerate shells separated by the shell mean level spacing $\Delta E_{\text{shell}} \approx 4$ meV (see [20], section 1.1), approximately constant for the shells I-VII depicted in Fig. 1(b).

As V_G is raised towards more negative values, the contact p-n junctions become more transparent [18], resulting in a gradual enhancement of the conductance close to the saturation limit. For the highest tunnel couplings, reached for the shells I and II, the conductance is greatly enhanced for all partial shell fillings due to the SU(4) Kondo effect, resulting in Kondo ridges in the middle of the $N = 1h, 2h$ and $3h$ Coulomb diamonds [18]. However, as T_K decreases for the next shells, the zero-bias conductance at half filling is gradually quenched in such a way that zero bias Kondo ridges are observed for odd numbers of holes only (Fig. 1(b)). This behavior is confirmed by the T -dependence of the zero bias conductance with gate voltage, depicted in Fig. 1(c), showing a decreasing conductance with lowering temperature at half filling of the shells III-VII, in opposite behavior to the shells I-II. As we will demonstrate by cotunneling level spectroscopy, the disappearance of the SU(4) Kondo effect is caused by significant splittings of the even hole energy spectrum, in the absence of disorder induced orbital mixing, preventing spin-orbital level degeneracies to form for even number of holes.

We first discuss the level spectrum and the evolution of the Kondo resonance for $N = 1h$ under parallel magnetic field B_{\parallel} in shell VI, corresponding to about 20 holes trapped in the valence band (Fig. 2(a)). The Kondo peak mainly splits according to two most visible peaks, highlighted by the dashed black lines in Fig. 2(a), evolving in B_{\parallel} with significantly different dV_{sd}/dB_{\parallel} slopes, in good agreement with an energy level spectrum including the curvature induced SOI (Fig. 2(d)). The $N = 1h$ states at $B_{\parallel} = 0$ consist in a pair of Kramers doublets formed by spin-orbital states with an antiparallel alignment of the orbital and spin magnetic moments [6] [namely $\{|K \downarrow\rangle, |K' \uparrow\rangle\}$ for the lowest doublet, and $\{|K \uparrow\rangle, |K' \downarrow\rangle\}$ for the highest one], that is split by the effective spin-orbit gap Δ_{SO} . Turning on the B_{\parallel} -field separates the two energy doublets into four spin-

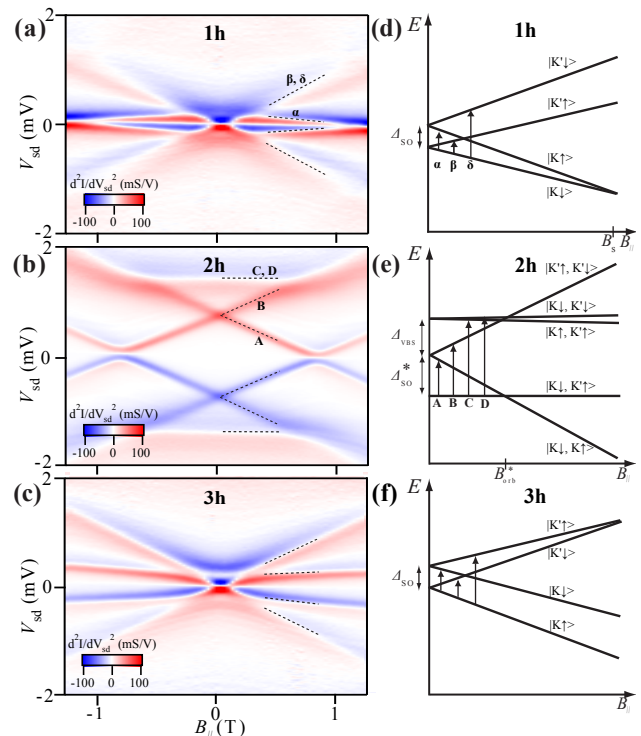


FIG. 2. (color online). (a-c) Current second derivative d^2I/dV_{sd}^2 versus bias voltage V_{sd} and axial magnetic field B_{\parallel} in the middle of the $N = 1h, 2h$, and $3h$ charge states of the shell VI. (d-f) Schematic representation of the expected low energy spin-orbital levels as a function of B_{\parallel} , corresponding to (a-c).

orbital states with slopes proportional to either $g_{orb} \pm g_s$ or $-g_{orb} \pm g_s$, with $g_{orb} \gg g_s$ the orbital and spin g -factors respectively [24]. This one-hole level scheme results in three B_{\parallel} -field dependent excitations [10], denoted α , β and δ in Fig. 2(d). The transitions are better resolved by plotting in Figs. 2(a-c) the second derivative of the current, d^2I/d^2V_{sd} , noting that the excitations correspond to lines of either extrema or zeros, depending on the degree of renormalization of the cotunneling processes at play [25]. Extrapolating the conductance peak associated to α at $B_{\parallel} = 0$ in Fig. 2(a) gives the amplitude of the effective spin-orbit splitting $\Delta_{SO} \approx 0.24$ meV for $N = 1h$, which is of the same order of magnitude than previous findings [6, 7, 10]. The energy dependence of the conductance peak associated to α also results in a SU(2) Kondo effect at the finite parallel magnetic field $B_s = \Delta_{SO}/g_s\mu_B$ due to the B_{\parallel} -field induced level crossing for $N = 1h$. The other main visible conductance peak in Fig. 2(a) takes into account the two other expected β and δ excitations (Fig. 2(d)), which are difficult to separate spectroscopically because of the tunnel-induced broadening of the two associated conductance peaks [14]. The large and positive slope of dV_{sd}/dB_{\parallel} for β and δ , roughly proportional to g_{orb} , reveals the dominant contribution from the orbital g -factor. In contrast,

the dependence in g_{orb} drops for the α transition, leading to a weak and negatively dispersing transition line in the conductance due to the spin Zeeman effect only, as indeed expected from the level spectrum of Fig. 2(d).

The $N = 3h$ theoretical energy level spectrum (Fig. 2(f)) is expected to be equivalent to the $N = 1h$ one (Fig. 2(d)) by just exchanging the two doublets at $B_{\parallel} = 0$ [10] (particle-hole symmetry), and indeed the measurement of Fig. 2(c) is in good agreement with the level scheme of Fig. 2(f). We find here a spin-orbit gap $\Delta_{SO} \approx 0.23$ meV, very close to the value measured for $N = 1h$ ($\Delta_{SO} \approx 0.24$ meV). Contrary to the situation with a single hole, we note the absence of B_{\parallel} -field induced crossing at low-energy due to the different $N = 3h$ level scheme [10, 15, 16].

After considering the SOI level structure for $N = 1h$ and $3h$, we now examine the situation at half shell filling ($N = 2h$), depicted in Figs. 2(b,e). The $N = 2h$ energy states can be readily built from linear combinations of the single hole states, leading to six independent configurations. At $B_{\parallel} = 0$, the singlet-like ground state (denoted $|K \downarrow, K' \uparrow\rangle$ in Fig. 2(e)) corresponds to the two holes occupying the low-energy Kramers doublet, and sets the origin of the cotunneling excitations [10]. The four excitations, denoted A, B, C and D in Figs. 2(b,e) refers to the transitions from the ground state to the first four excited states where only one hole lies in the high-energy Kramers doublet. The expected sixth state ($|K \uparrow, K' \downarrow\rangle$) is not visible experimentally in Fig. 2(b) [10] since it would imply simultaneous spin flips of both holes. The excitations (A, B) appear as dI/dV_{sd} conductance steps (peaks in d^2I/dV_{sd}^2 of Fig. 2(b)), with $|dV_{sd}/dB_{\parallel}|$ average slopes given by the orbital Zeeman effect. We deduce here an orbital g -factor $g_{orb} \approx 15.5 \pm 0.5$ (equivalently an orbital magnetic moment $\mu_{orb} = g_{orb}\mu_B/2 = 0.45$ meV.T $^{-1}$), in agreement with the B_{\parallel} -field orbital splittings of $N = 1h$ and $3h$ (Figs. 2(a,c)). The excitations (C, D) merge together into an enhanced dI/dV_{sd} Kondo peak at finite bias [25], such as both excitations cannot be separately distinguished under the B_{\parallel} -field. At $B_{\parallel} = B_{orb}^* = \Delta_{SO}^*/g_{orb}\mu_B$ (see below for the definition of Δ_{SO}^*), a singlet/triplet-like level crossing occurs [17], leading to a new ground state configuration for $B_{\parallel} > B_{orb}^*$. From the avoided level crossing between the $|K \downarrow, K \uparrow\rangle$ and $|K \downarrow, K' \uparrow\rangle$ states at B_{orb}^* in Fig. 2(b), we estimate a very weak disorder-induced valley mixing ($\Delta_{KK'} \approx 0.04$ meV), in contrast to previous cotunneling studies [10, 21], where disorder was largely dominating the SOI. Our measurements therefore complement sequential tunneling spectroscopies in the ultra-clean regime [7].

One striking observation made in our device is the huge effective SOI splitting for $N = 2h$, $\Delta_{SO}^* \approx 0.75$ meV in Figs. 2(b,e), as defined by the energy of the first excitations at $B_{\parallel} = 0$. This strong value cannot be accounted for the curvature induced SOI only (Δ_{SO}

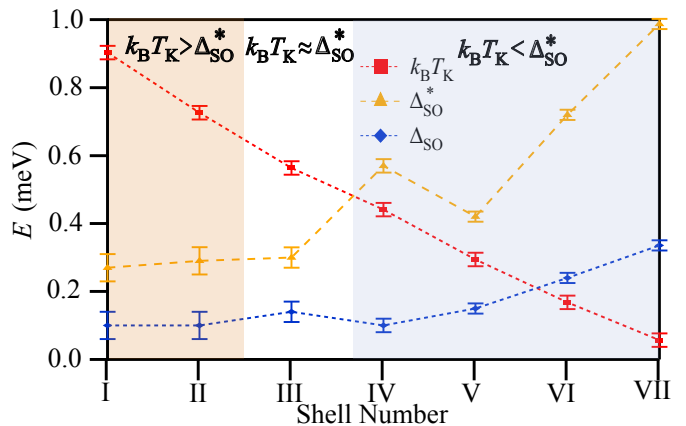


FIG. 3. (color online). Evolution of Kondo temperature T_K , one-hole spin-orbit gap Δ_{SO} and two-hole effective gap Δ_{SO}^* for the shells I-VII.

$\approx \Delta_{SO}^*/3$) since the latter is mainly related to the specific CNT bandstructure and thus evolves continuously from odd to even valleys [10]. Here, the enhancement of Δ_{SO}^* with respect to Δ_{SO} probably originates from short range Coulomb interactions, well visible at half shell filling. More specifically, recent theoretical studies [26–28] underlined the important role of Coulomb inter-valley backscattering (VBS) processes, resulting in an additional lifting of degeneracies in the spin-orbit level structure. This interpretation is indeed confirmed by the significant effective splitting $\Delta_{VBS} \approx 0.67$ meV of the excited quadruplet [26, 28], associated to the transitions (A, B) and (C, D), regrouped into two energy doublets at $B_{\parallel} = 0$, depending whether the two holes have equal or opposite isospins. While the sign of this interaction is in good agreement with previous observation [7], the large magnitude of the effective Δ_{VBS} is dramatically larger in our experiment ($\Delta_{VBS} \approx 0.19$ meV in Ref. [7]). Our observations put strong challenges for current theoretical works [26–28], and suggest possible neglect of many-body effects related to screening processes, since the quantitative determination of exchange constants is a notoriously difficult problem [29, 30].

After identifying the influence of the SOI in the energy level structure of a given hole shell (Fig. 2), we now show its consequence on the Kondo effect seen in Fig. 1. Figure 3 depicts the amplitudes of Δ_{SO} and Δ_{SO}^* , measured respectively for the $N = 1h$ and $2h$ partial shell fillings, in the seven available shells of Fig. 1(b). The magnitude of the SOI gap Δ_{SO} increases with decreasing gate voltage from the shells I to VII, as expected for curvature induced SOI in the valence band [10, 31]. Interestingly, Δ_{SO} and Δ_{SO}^* follow a comparable gate dependence, with a ratio $\Delta_{SO}^*/\Delta_{SO} \approx 3$ that is approximately constant for all shells considered in Fig. 3 (except for shell IV). For the successive hole shells, the effective SOI gap Δ_{SO}^* is compared with the Kondo temperature

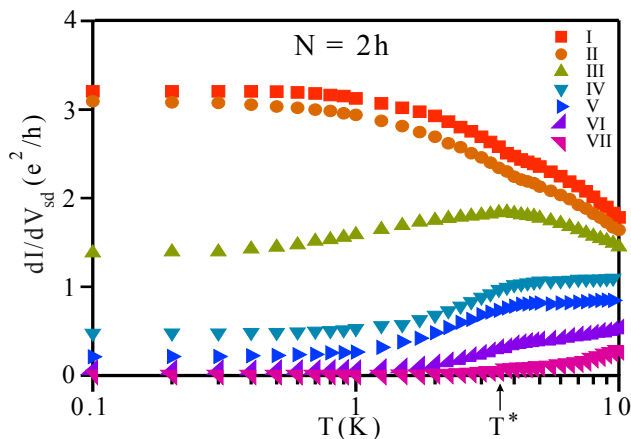


FIG. 4. (color online). Zero bias differential conductance dI/dV_{sd} versus T in the center of even hole diamonds ($N = 2h$) in the successive shells (I-VII), from $T = 100$ mK up to 10 K.

T_K , estimated from the half width at half maximum of the dI/dV_{sd} versus V_{sd} curves, recorded in the middle of the $N = 1h$ diamond (see Fig. 3). We find that the Kondo temperature gradually decreases from the shells I to VII, in agreement with the evolution of the U/Γ ratios with the gate voltage. The opposite evolutions of the Kondo temperature and the SOI with V_G (Fig. 3) explain now the different transport regimes previously seen in Fig. 1, depending whether Kondo or spin-orbit physics prevail, as we discuss now.

The competition between Kondo and SOI in the two-hole sector is better seen by the full dependence of the conductance versus temperature for all shells in Fig. 4. For the first two $N = 2h$ shells, the conductance saturates at $T < T_K$ up to 3.1 - $3.2 e^2/h$, close but below the unitary limit $4 e^2/h$. Due to the high conductance for odd valleys ($dI/dV_{sd} \approx 2e^2/h$), see Fig. 1c, we can rule out source-drain asymmetries of the tunnel barriers to explain this reduction of conductance. In addition, orbital asymmetries of the tunnel couplings [21, 32] also are unlikely here, due to the clearly-evidenced weak disorder in our sample. Thus, we can attribute the weakly broken SU(4) Kondo state in shells I-II to the small but sizeable (in comparison to T_K) effective spin-orbit coupling Δ_{SO}^* , as seen in Fig. 3. This interpretation is confirmed by the next two-hole shell III, where the renormalized SOI and Kondo energies become comparable and compete, resulting in a marked drop of conductance down to $1.4 e^2/h$ at low temperature. This rapid but not total quenching of the SU(4) Kondo effect is in qualitative agreement with theoretical expectations [16], and results for the shell III in a conductance maximum ($dI/dV_{sd} \approx 1.9 e^2/h$) at the temperature $T^* \approx \Delta_{SO}^*/k_B$. By further weakening the Kondo temperature in shells IV-VII, one observes a complete suppression of the Kondo effect (cotunneling regime), with a purely monotonous T -

dependence of the conductance, due to the predominance of orbital splitting which totally remove the degeneracies in the system. Our ultraclean CNT with sizeable tunnel couplings to the metal leads thus offers a complete span from SU(4) to SU(2) behavior in a single device.

In conclusion, we have revealed strong spin-orbit physics in ultraclean carbon nanotube from cotunneling spectroscopy, leading to a rich competition with the Kondo effect. Our results are in agreement with theoretical predictions [16, 17], if one takes into account renormalizations of the spin-orbit interaction for two-hole filling. Disorder-free nanotubes may come one day close to model systems, but our measurements indicate that more theoretical work beyond the present state-of-the-art [26, 27] is still needed towards a complete microscopic understanding.

We thank C. Balseiro, V. Bouchiat, P. Cornaglia, S. De Franceschi, M.-B. Lepetit, M. Rontani, and G. Usaj for valuable discussions, E. Eyraud, R. Haettel, D. Lepoitevin for technical support, J. L. Tomassin, H. Haas, T. Meunier for help in the device fabrication, and C. Thirion, E. Bonet, R. Piquerele for the data acquisition software development. Devices were fabricated in the PTA (CEA/CNRS) facility. This work is financially supported by ANR-PNANO project Mol-NanoSpin No ANR-08-NANO-002, and ERC Advanced Grant Mol-NanoSpin No 226558.

-
- [1] N. Hamada, S. I. Sawada, and A. Oshiyama, Phys. Rev. Lett. **68**, 1579 (1992).
 - [2] S. Sahoo, T. Kontos, J. Furer, C. Hoffman, M. Graber, A. Cottet, and C. Schonenberger, Nature Phys. **1**, 99 (2005).
 - [3] M. Urdampilleta, S. Klyatskaya, J. P. Cleuziou, M. Ruben, and W. Wernsdorfer, Nature Mat. **10**, 502 (2011).
 - [4] H. O. H. Churchill, A. J. Bestwick, J. W. Harlow, F. Kuemmeth, D. Marcos, C. H. Stwertka, S. K. Watson, and C. M. Marcus, Nature Phys. **5**, 321 (2009).
 - [5] F. Pei, E. A. Laird, G. A. Steele, and L. P. Kouwenhoven, Nature Nanotech. **7**, 630 (2012).
 - [6] F. Kuemmeth, S. Ilani, D. C. Ralph, and P. L. McEuen, Nature(London) **452**, 448 (2008).
 - [7] S. Pecker, F. Kuemmeth, A. Secchi, M. Rontani, D. C. Ralph, P. L. McEuen, and S. Ilani, Preprint at arXiv:1302.1877 [cond-mat.mes-hall] (2013).
 - [8] T. Ando, J. Phys. Soc. Jpn. **69**, 1757 (2000).
 - [9] D. H. Hernando, F. Guinea, and A. Brataas, Phys. Rev. B. **74**, 155426 (2006).
 - [10] T. S. Jespersen, K. Grove-Rasmussen, J. Paaske, K. Muraki, T. Fujisawa, J. Nygard, and K. Flensberg, Nature Phys. **7**, 348 (2011).
 - [11] S. Florens, A. Freyn, N. Roch, W. Wernsdorfer, F. Balestro, P. Rourra-Bas, and A. A. Aligia, J. Phys. Condens. Matter. **23**, 243202 (2011).
 - [12] M. S. Choi, R. Lopez, and R. Aguado, Phys. Rev. Lett. **95**, 067204 (2005).

- [13] F. B. Anders, D. E. Logan, M. R. Galpin, and G. Finkelstein, *Phys. Rev. Lett.* **100**, 086809 (2008).
- [14] P. Jarillo-Herrero, J. Kong, H. S. J. van der Zant, C. Dekker, L. P. Kouwenhoven, and S. de Franceschi, *Nature (London)* **434**, 484 (2005).
- [15] A. Makarovski, A. Zhukov, J. Liu, and G. Finkelstein, *Phys. Rev. B* **75**, 241407(R) (2007).
- [16] M. Galpin, F. Jayatilaka, D. Logan, and F. Anders, *Phys. Rev. B* **81**, 075437 (2010).
- [17] T. Fang, W. Zuo, and H. Luo, *Phys. Rev. Lett.* **101**, 246805 (2008).
- [18] A. Makarovski, J. Liu, and G. Finkelstein, *Phys. Rev. Lett.* **99**, 066801 (2007).
- [19] J. Nygard, D. H. Cobden, and P. E. Lindelof, *Nature (London)* **408**, 342 (2000).
- [20] Supplementary Material accompanies this paper. It can be downloaded at ...
- [21] K. Grove-Rasmussen, S. Grap, J. Paaske, K. Flensberg, S. Andergassen, V. Meden, H. I. Jorgensen, K. Muraki, and T. Fujisawa, *Phys. Rev. Lett.* **108**, 176802 (2012).
- [22] J. Cao, Q. Wang, D. Wang, and H. Dai, *Small* **1**, 138 (2005).
- [23] J. P. Cleuziou, W. Wernsdorfer, V. Bouchiat, T. Ondarcuhu, and M. Monthieux, *Nature Nanotech.* **1**, 53 (2006).
- [24] E. D. Minot, Y. Yaish, V. Sazonova, and P. L. McEuen, *Nature (London)* **428**, 536 (2004).
- [25] J. Paaske, A. Rosch, P. Wolffe, N. Mason, C. M. Marcus, and J. Nygard, *Nature Phys.* **2**, 460 (2006).
- [26] A. Secchi and M. Rontani, *Phys. Rev. B* **80**, 041404(R) (2009).
- [27] B. Wunsch, *Phys. Rev. B* **79**, 235408 (2009).
- [28] A. Secchi and M. Rontani, Preprint at arXiv:1306.3502 [cond-mat.mes-hall] (2013).
- [29] K. Handrick, J. P. Malrieu, and O. Castell, *J. Chem. Phys.* **101**, 2205 (1994).
- [30] M. B. Lepetit, *Recent Research Developments in Quantum Chemistry*, Vol. 3 (2002) p. 143.
- [31] T. S. Jespersen, K. Grove-Rasmussen, K. Flensberg, J. Paaske, K. Muraki, T. Fujisawa, and J. Nygard, *Phys. Rev. Lett.* **107**, 186802 (2011).
- [32] G. Kirsanskas, J. Paaske, and K. Flensberg, *Phys. Rev. B* **86**, 075452 (2012).